Towards Differential Magnetic Force Sensing for Ultrasound Teleoperation

David Black
Dept. of Electrical and Computer Eng.
University of British Columbia
Vancouver, Canada
dgblack@ece.ubc.ca

Amir Hossein Hadi Hosseinabadi
Dept. of Electrical and Computer Eng.
University of British Columbia
Vancouver, Canada
amirhossein.hadi@gmail.com

Nicholas Rangga Pradnyawira
Dept. of Mechanical Engineering
University of British Columbia
Vancouver, Canada
nicholasrangga010303@gmail.com

Maxime Pol
École de l'Air et de l'Espace
École Polytechnique
Paris, France
maxime.pol@ecole-air.fr

Mika Nogami
Integrated Engineering Program
University of British Columbia
Vancouver, Canada
mikanogami@gmail.com

Tim Salcudean
Dept. of Electrical and Computer Eng.
University of British Columbia
Vancouver, Canada
tims@ece.ubc.ca

***Abstract*—Low-profile, low-cost force/torque sensing is important in many applications. It can enable haptic feedback, performance evaluation, training, data collection, and teleoperation of ultrasound procedures. In this paper we introduce a new concept of differential magnetic field based multi-axis force sensing. A magnet is separated from two adjacent Hall effect sensors by a flexible suspension. The differential signal from the two sensors allows precise deflection measurement, and combining several of these on a compliant structure enables multi-axis force sensing. The concept is motivated, described, simulated, and tested. In initial experiments, the best-case deflection resolution is found to be 856 nm, with full-scale range of 1.5 mm and a root-mean-square force/torque error of 10.37% compared to an off-the-shelf sensor. This paper demonstrates the feasibility and potential of this force sensing mechanism.**

***Index Terms*—Force Sensing, Hall Effect, Teleoperation, Human Computer Interaction**

I. Introduction

Ultrasound (US) probe force/torque sensing is useful for a number of applications. Force is an important parameter to control in US, as it determines image quality and what structures are visible. Additionally, to make teleoperation intuitive and realistic for the operator, haptic feedback is essential. Force sensing is thus important in robotic teleoperation of US procedures [1], [2], [3], [4], [5], or for "teleoperating" novice people in performing exams [6], [7]. Furthermore, US involves relatively large forces which lead to increased musculoskeletal injury in sonographers [8] and discomfort for patients, which could be reduced through safety monitoring with a force sensor. Additionally, for US tele-guidance [9], [10], training [11], [12], and skill assessment [13], the applied forces would be valuable. Finally, autonomous robotic US requires force control [14], [15], and for learning-based approaches to robotic or AI-guided US, data including forces must first be collected during procedures [16], [17].

However, sensing forces on an US probe is not trivial. Sonographers do not want excessive additional weight, bulk, or cable pull, and the sensor cannot be placed between the probe and the patient as it would disrupt image formation. Several groups have instrumented US probes by placing an off-the-shelf (OTS) sensor between the probe and an external shell which is gripped by the user [2], [18], [19], [20], [21]. However, this approach makes the probe bulky and hard to grasp. Because the force sensor cannot easily be placed near the US transducer array, it often requires high torque capability, leading to limited availability and high cost. Huang et al. placed small piezoresistive pressure pads on either side of the US probe face [22], but this does not give sufficient force information and may interfere with the imaging. Most of the aforementioned robotic US systems simply have a force sensor between the robot end-effector and the US probe, which is of course infeasible for manual US.

We therefore set out to design a low-profile, low-cost, easy-to-manufacture sensing solution for US to enable force feedback and control in US teleoperation, as well as the many other applications. The design objectives are outlined in Section I-A. There are many potential sensing modalities, reviewed in [23], [24]. These include piezoresistive pads [25], strain gauges, elastomeric transducers [26], capacitive sensing, and optical deflection sensing [27]. Each modality was evaluated thoroughly and/or tested physically, but each had issues. Namely, optical sensing requires costly precision fabrication to align the slit with the LED and photodiode, and the components and electronics take up more space than is desirable around an US probe [28]. Strain gauges require careful preparation, material choice, and fabrication of the flexure, leading to increased cost and complexity [29]. Moreover, installation and removal would likely be difficult, which would slow down the cleaning of the US probe between cases. Elastomeric transducers are not readily available [30], and piezoresistive pads require exact pre-load to ensure all axes are contacting properly at all times (i.e. they cannot measure negative pressures). We tested several models which showed large hysteresis and inter-axis coupling,

979-8-3503-9993-6/23/$31.00 © 2023 IEEE

2023 IEEE World Haptics Conference (WHC)
WHC 2023, Delft, Netherlands, July 10–13, 2023

making fabrication and resolving of separate forces difficult. Preliminary tests integrating small, single axis load cells (Honeywell FSAGPDXX001RCAB5 and MAMSDXX025WCSC3) into a 3D printed shell proved ineffective for the same reasons. Capacitive sensing is more precise than necessary for this application, and involves more complex electronics and careful fabrication [23].

Hall effect sensors have also seen limited use for force measurement. Most papers place a sensor near a magnet on a compliant structure such as the finger tip of a robotic grasper to sense when a single-axis force is applied [31], [32]. An ingenious human finger tip force sensor is described in [33], but it is very specifically applicable only to a human finger. Finally, a 3-axis force sensor with Hall effect sensors and magnets is designed in [34]. This axially offsets a single Hall effect sensor from a magnet. To achieve sufficient signal, it relies on large displacements and thus cannot be miniaturized. Indeed, the presented device is very large and heavy. Additionally, the full-scale range is very small and the response is not linear.

Instead, in this paper we present a novel multi-axis force sensing approach based on Hall effect sensors in a differential configuration. The solution is a low profile, modular, optimizable, and customizable force sensor for applications involving a relatively soft environment, such as US and human-robot interaction. The primary design considerations are listed in Section I-A before detailing the differential magnetic force sensing method in Section I-B. The physical principles are outlined in Section II-A and used in simulation to design a sensor. Next, the sensing technique is evaluated through experiments of the deflection sensing capabilities, resolution, noise, and planar 3-axis force/torque calibration and measurement in Sections II-B and III. Finally, several modifications and improvements for future work are proposed in Section IV.

A. Design Objectives

For force sensing during US procedures, several design objectives must be met. The sensing should be

1) As low profile, small, and light as possible
2) Easy to install and remove for cleaning
3) Sufficiently accurate and precise - the human hand's just noticeable difference (JND) for force sensing is 7%, with an applied force resolution of 0.36 N [35]. The force sensor should be at least this good. Performing much better is pointless as the user will not notice a difference.
4) Sufficiently fast - as this sensor is intended primarily for human-robot interaction, its performance should at least match a human. The human hand bandwidth for generating forces is approximately 20-30 Hz [36]. In US, the contact is soft and low bandwidth. However, contacting stiff structures such as bones can lead to higher frequencies. Human hand perception has a bandwidth of up to 250 Hz [37]. For Nyquist-Shannon sampling, a bandwidth of 500 Hz is thus aimed for.
5) Wireless - point of care US (POCUS) probes are often wireless, and cable pull disrupts sonographers.
6) Inexpensive - POCUS probes are only several thousand US dollars, making US an increasingly popular modality, especially in under-resourced communities where human teleoperation could be important. The force sensor should not add significantly to the cost. (Current quality OTS sensor cost is similar to a POCUS device.)

B. Hall Effect-Based Force Sensing

Given a Hall effect sensor lying on a horizontal surface, moving a magnet towards or away from the sensor will vary the output voltage. Though the sensor is linear with respect to magnetic field, the magnetic field changes non-linearly with distance. Furthermore, moving the magnet in either horizontal direction will also vary the field, and the dynamic range will not be great since the magnetic field decreases rapidly with distance and is affected by noise. Hence, a single-sensor, single-magnet axial setup is not suitable for precise deflection measurement.

Instead, suppose we add a second Hall effect sensor adjacent to the first, with a cylindrical permanent magnet held vertically above them, centred between the two sensors. If the axis of the magnet is aligned vertically (z axis), parallel to the sensitive axis of the sensors, both sensors read the same magnetic field, so their difference is zero. Moving the magnet slightly side to side across the sensors (x axis) alternately increases or decreases the measurement of one of the sensors while doing the opposite to the other. The difference between the readings thus grows in magnitude further from the centre, and its sign depends on the direction of motion. As demonstrated in Section II-A, for relatively small displacements from centre, the proportional change is approximately linear in distance. Hence, we have a linear single axis deflection sensor. This is illustrated in Fig. 1.

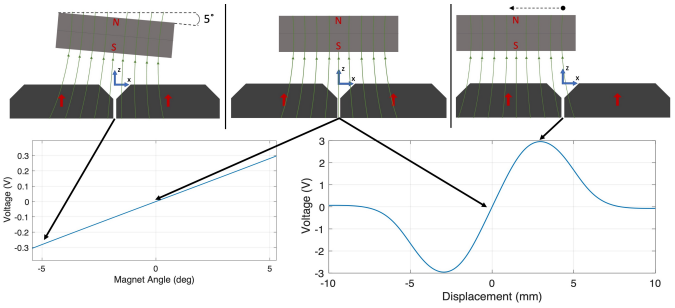

Fig. 1. Differential magnetic displacement sensing concept and simulation results. As the magnet moves across the Hall effect sensor pair, the differential voltage output varies (bottom right). In a centered position, the difference cancels all other DOFs except the rotation shown on the left.

When the magnet is centered on the sensors, moving it axially away from the sensors decreases both sensor readings by an equal amount, so the differential signal is zero. Similarly, translations in y and rotations about x and z have 0 response. Rotations about y have a linear differential response as shown in Fig. 1, but this rotation is limited to $\ll 1^\circ$ when the sensors are built into a shell on an US probe. The voltage response is thus two orders of magnitude smaller than that

in the x direction. Therefore, the sole appreciably sensitive axis of this configuration is the x translation, which is used for measurement. Though most axes in isolation have no voltage response, they can affect the x response. As indicated, angular changes are very small, but the effect of axial and lateral translations are shown in Fig. 6. These coupling effects can be calibrated out by using more than one sensor pair in different orientations. A further advantage of the differential pair reading is that any external noise sources tend to cancel out. By placing an analog to digital converter (ADC) as close as possible to the sensors and adding a low pass filter, we can additionally avoid electronic noise from long wires.

With the ability to measure small deflections, a magnet can be embedded in a thin shell around an US probe, and a Hall effect sensor pair placed on the probe, opposite the magnet. With ≥ 6 of these sensing modules around the probe and a compliant suspension between probe and shell, it should be possible to measure the 6 axis force and torque applied to the probe. As the magnets and Hall effect sensors are very small and only need to be spaced apart by 1-2 mm, the shell can be very low profile. Furthermore, some misalignment can be tolerated simply by biasing the sensors. Hence, conceptually a magnetic field-based force sensing approach seems promising for US probe force measurement and likely other applications. We refer to this system as differential magnetic force/torque sensing (DMFS).

II. Methods

A. Simulation

Numerical simulations were used for initial evaluation of the feasibility of DMFS and to guide the design of the first prototype. Specifically, we sought a linear response with good dynamic range, as well as easy-to-obtain, small, and inexpensive components. To this end, the design parameters in Table I were considered. To determine these factors, we wrote a simulation in MATLAB to calculate the voltage output of two Hall effect sensors as the magnet position moves, as a function of the design parameters.

Note that NdFeB is neodymium-iron-boron. The Hall elements of the sensors are 2 mm away from the edges of the sensors, so 4 mm spacing is achieved by placing the sensors directly adjacent to each other. Given that the field curves back around the magnet, it is conceivable that the sensors should be placed at an angle for optimal sensitivity. However, it was found that flat sensors, parallel to the magnet give best performance and lowest profile. The deflection range was chosen to fill the linear range of the voltage response (Fig. 1). A larger deflection would feel softer for the user and would require both a larger magnet and axial offset to increase the linear range, which would make the sensor more bulky.

Hall effect sensors measure magnetic flux density. The field strength of a permanent cylindrical magnet is given in [38], equations 3 to 10 by modeling a permanent magnet as a sheet of current wrapped around a cylinder. By aligning the sensitive axis of a Hall effect sensor parallel with the north-south magnet axis, the radial component of the field can be ignored, and the relevant axial component is, as a function of axial distance, z, and radial distance, ρ:

TABLE I
Design parameters and values chosen from simulations

Parameter	Chosen Value
Sensor sensitivity	25 mV/mT
Sensor spacing	4 mm
Sensor angle	Parallel
Magnet radius	6.35 mm
Magnet length	1.59 mm
Magnet type	NdFeB, N48 grade
Axial offset	1 mm
Desired deflection range	$\pm 1 - 1.5$ mm

$$B_z = \frac{B_0 r}{r+\rho}\left[\frac{z_+ C_+}{\sqrt{z_+^2 + (\rho+r)^2}} - \frac{z_- C_-}{\sqrt{z_-^2 + (\rho+r)^2}}\right] \quad (1)$$

Where r is the radius of the magnet and 2ℓ is the length. The values $C_\pm$ are computed by solving an integral which depends on $k_\pm$ and γ where

$$k_\pm = \sqrt{\frac{z_\pm^2 + (\rho - r)^2}{z_\pm^2 + (\rho + r)^2}}$$
$$\gamma = \frac{r-\rho}{r+\rho}$$

and $z_\pm = z \pm \ell$. See details and derivation in [38]. Determining a clear analytical functional dependence of B_z on ρ and z is difficult. We thus wrote a MATLAB script to compute the values numerically for all points along the trajectory of a magnet moving across the sensor pair. Additionally, the difference between the two simulated sensors' readings was computed.

It was found the Texas Instruments DRV5056-Q1 with 25 mV/mT sensitivity and 158 mT range best satisfied the requirements. Sensors with up to 200 mV/mT sensitivity are available but give proportionally less range. The magnet details are found in Table I. With this configuration, the differential response was highly linear for ± 1.5 mm deflections, which correspond to ± 1.5 V outputs, depending on the axial offset. The R^2 value in this range is 0.999. Beyond ± 2 mm it quickly becomes less linear.

The simulation was verified by placing the selected magnet on a linear stage and stepping it across two Hall effect sensors with 1.5 mm offset. The result is shown, together with the theoretical calculation, in Fig. 2.

B. Experiments

With a configuration designed through simulation and verified with a simple test, we mounted Hall effect sensors in the desired orientation on a printed circuit board (PCB). The analog output was passed through a second order passive RC low-pass filter to a 13-bit ADC with two input channels. The filter component values were 68 $k\Omega$ and 2.2 nF, giving a -3 dB frequency of approximately 685 Hz. This is relatively high to allow high bandwidth force changes such as suddenly

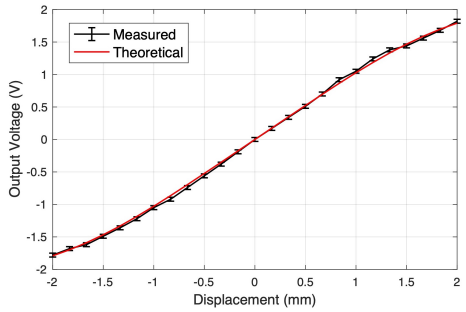

Fig. 2. Theoretical and measured differential voltage output at 1 mm axial offset

contacting a relatively stiff surface. The ADC output was sent to an Arduino Mega using serial peripheral interface (SPI).

1) Position Test: A single sensing module was fastened to the end of a 3D printed polylactic acid (PLA) extension mounted to a manual 3-axis linear stage on an optical prototyping table. The stage resolution was 0.002 mm. A magnet was attached to the end of a second PLA extrusion facing the Hall effect sensors, mounted on a rotating disk on the prototyping table. Using 3D printed pegs on the magnet side and holes on the sensor side, the stage was adjusted and the magnet was rotated so the magnet and sensor were parallel and the magnet was aligned in the centre between the two sensors. The setup is shown in Fig. 3. The long PLA extrusions avoid magnetic field artifacts from the large metal components.

With this setup, the Hall effect sensor outputs were measured for displacement sweeps across the Hall effect sensor pair at axial offsets of 0.5, 1.0, 1.5, 2.0, and 2.5 mm, and lateral offsets of 0.0, 0.5, 1.0, and 1.5 mm from centre. Across the sensor pair, the displacement was measured in 0.1 mm increments. Additionally, several long measurements were recorded with no motion to characterize the noise.

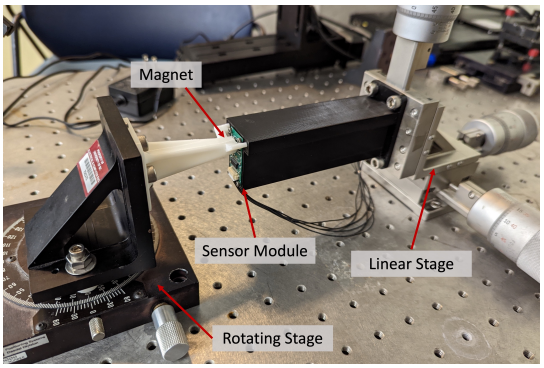

Fig. 3. Setup for single sensor characterization

2) 3-DOF Force Sensing: As a proof-of-concept for the force sensing utility of the DMFS concept, a 3-DOF planar jig was built. With this device, horizontal forces in two axes (x and y), and the in-plane torque about the vertical axis (z) could be applied and measured. The jig consisted of an inner square and an outer square with a gap between the two.

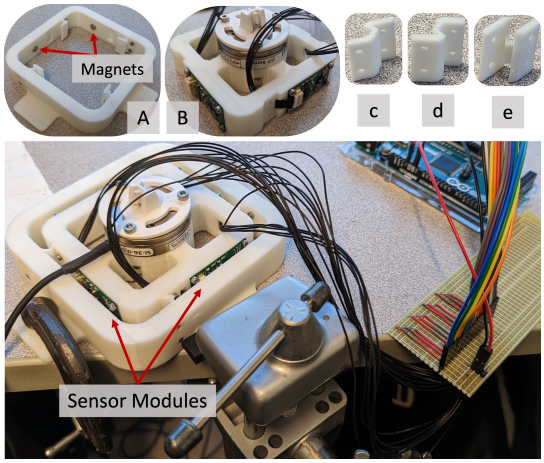

Fig. 4. Setup for single sensor characterization. A: Outer shell with suspension elements in place. B: Inner square with sensors. C, D, E: Stiff, medium, and soft suspension elements. To facilitate debugging in this prototype, all sensor modules were wired in parallel. In reality, the wiring would be a bus of 5 wires shared by all the modules, and only a single separate wire for each.

Thin, bent arms were mounted between the two squares as a compliant suspension. All parts were 3D printed with a PLA fused deposition modeling (FDM) printer (Afinia H800+), with 0.15 mm layer thickness, and 0.1 mm horizontal resolution. The inner and outer square were made with 10 mm thick walls to avoid flexing. The jig was printed vertically so forces and torques in the horizontal plane were not subject to the anisotropic nature of the material across the printed layers.

Precisely-positioned screw holes and mounting guides were included on the prints. In these positions, the three sensor modules were mounted on the inner square and corresponding magnets on the outer square, with 1.5 mm offset. An OTS force sensor (ATI Nano43) was mounted on the inner square with a handle for applying forces/torques. The outer square was clamped to a table while the inner square was elevated to avoid friction with the table. The test jig is shown in Fig. 4.

A random series of in-plane forces and torques was applied to the handle of the force sensor, up to approximately 25 N and 275 Nmm. The forces and torques measured by the OTS sensor were recorded with timestamps using a Python program, as were the differential voltages of the sensor modules. The sampling rate was 60 Hz, and the series were 2-3 minutes long. The process was repeated three times with different suspensions to see the effect of system stiffness on the force readings. First, a stiff suspension with full-height (20 mm high), 2 mm thick supports was used. Next, a medium suspension with full-height, 1.25 mm thick supports was used. A final test was carried out using 1.25 mm thick supports that were only 8 mm high to reduce stiffness further.

The OTS and DMFS sensor measurements were aligned in time using a sharp initial force, and interpolated linearly to match sample-for-sample. The first half of the samples of the three sensor modules were arranged as columns of a matrix, X, and augmented by a column of ones. The first half of the x-axis force (F_x), y-axis force (F_y), and z-axis torque (T_z)

from the OTS sensor were similarly placed in the columns of a matrix, Y. A 3×3 calibration matrix, C, was calculated such that $XC = Y$ using least squares; i.e. $C = (X^\top X)^{-1}X^\top Y$. The affine calibration was then applied to the second half of the data, X' and Y', and the error was computed as $X'C-Y'$.

III. Results

1) Position Test: The resulting differential voltage curves are shown in Fig. 5, color-coded and labeled by the axial offset. It is clear that the sensitivity decreases as the magnet moves further away from the sensors, since the slope decreases. On the other hand, the slope is not as strongly affected by the lateral offset. This is seen in Fig 6, which shows slope as a function of lateral and axial offset. The sensitivity at the chosen operating offset is 2.2 V/mm. Additionally, the R^2 value is close to 1 and only drops as axial displacement becomes very small, possibly due to saturation.

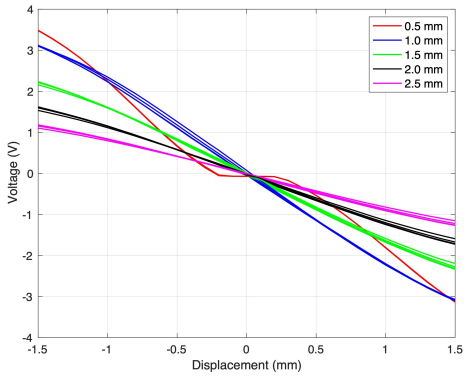

Fig. 5. Differential voltage versus displacement at different axial and lateral offsets. Color coding is by axial offset.

With the sensor stationary, 50000 samples were measured at 60 Hz. The samples were normally distributed with standard deviation of 0.93 mV. A 95% confidence interval of 2σ gives a best-case deflection resolution of 1.86 mV. The ADC (MCP3302) is 13 bits with 2's complement encoding, so the least significant bit is 1.2 mV. Thus, the 1.86 mV value is close to the theoretical resolution limit. This justifies not using a more expensive, higher resolution ADC, as the extra resolution would just be measuring noise. On the other hand, the ADC is not limiting the achievable resolution of the sensor. With the measured resolution and sensitivity, the positional resolution is $(0.00186V)/(2.2V/mm) = 0.846\mu m$. Assume we apply forces of ≤ 25 N, and design a suspension so the displacement at 25 N is 1.5 mm. Given the position resolution, the force resolution would be 0.0167 N in the ideal case.

2) 3-DOF Force Sensing: The measured forces are plotted in Fig. 7. As expected, the results are better with softer suspension, as more of the sensor's dynamic range is used so the signal to noise ratio is greater. The mean and standard deviations of the errors are shown in Table II.

The DMFS sensor modules have an operating range of ±1.5 mm. This corresponds to a 2.876 V range. With the stiff suspension, only 2-4% of this range was used. This

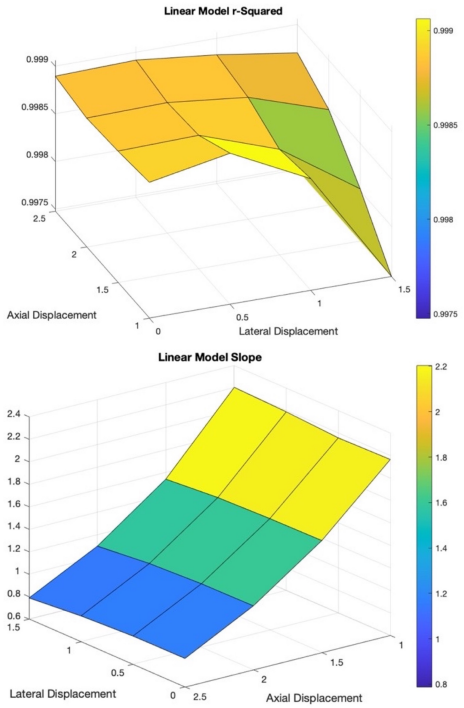

Fig. 6. Linearity (R^2; top plot) and sensitivity (slope; bottom plot) versus axial and lateral offset (mm).

TABLE II
Errors between DMFS and OTS sensors (mean $\pm$ standard deviation), and mean % error.

	Stiff	Medium	Soft
F_x	0.00 ± 1.96 N	0.015 ± 1.83 N	0.00 ± 1.77 N
F_y	-0.08 ± 3.77 N	0.002 ± 1.97 N	0.00 ± 1.68 N
T_z	0.82 ± 35.57 Nmm	0.68 ± 19.02 Nmm	0.00 ± 15.36 Nmm
%	20.62%	12.13%	10.37%

explains the worse performance. For the medium suspension, 20-45% of the range was used, and for the soft, 48-72% was used, corresponding to deflections of 0.72-1.1 mm, which still feels stiff in hand (the fingertip itself compresses more when gripping an object). We built an even softer suspension to use 100% of the dynamic range, but this led to issues of relatively large out-of-plane rotations which compromised the fidelity of the 3-DOF test. In a 6-DOF system, it would be feasible to take advantage of a softer suspension.

IV. Discussion

In this paper we have introduced a differential magnetic flux-based force sensor for low-profile, low-cost applications. We have tested its single-axis resolution and noise performance, and demonstrated its use as a 3-DOF force sensor. The sensor tracked the measurements of a commonly used OTS sensor with approximately 10% root mean square error, which is slightly above the human hand's 7% JND [35]. However, several factors can likely improve performance. First, the 3-DOF jig flexed slightly under the application of forces, so a stiffer material than PLA should be used for actual

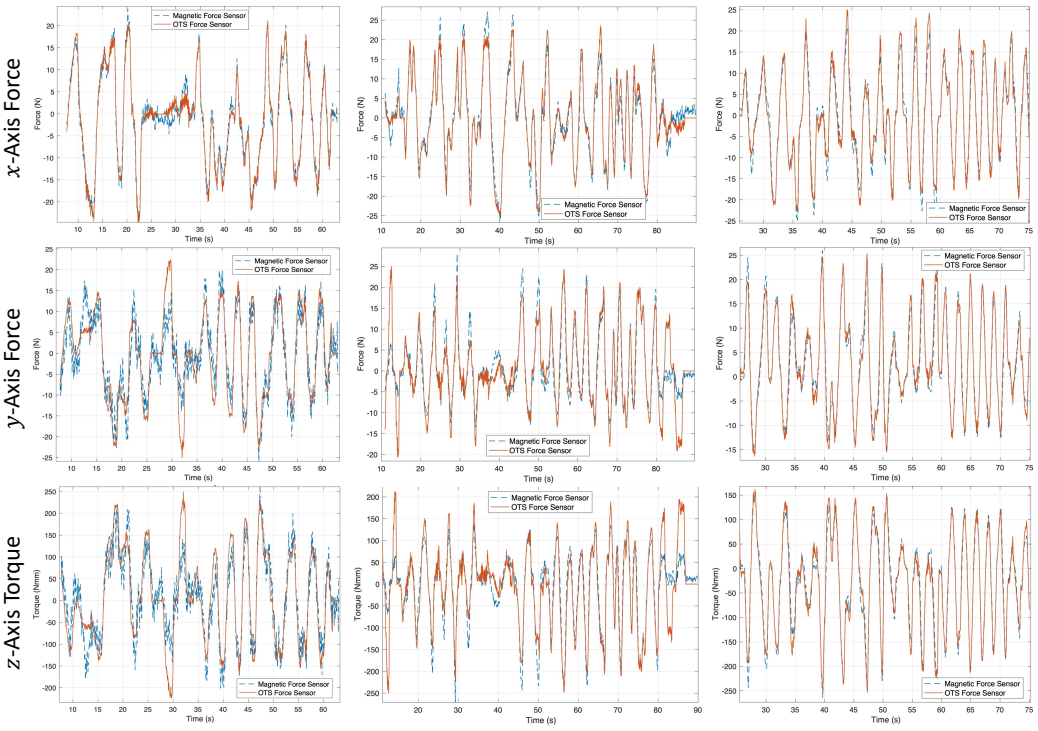

Fig. 7. Measured force from magnetic sensor (blue dotted) and OTS sensor (orange solid). Left column is with stiff suspension, middle is medium, and right is soft. The soft suspension leads to the best performance.

applications. Required screw hole tolerances led to occasional, sudden, slight slips of the suspension on the central square, leading to the infrequent sharp peaks at higher forces in Fig. 7. The forces applied at the top of the OTS force sensor caused moments about x and y as well, though no consequent deflections were visibly noticeable until we tried an even softer suspension. It is likely this had some effect on the data, though.

Additionally, the electronics and processing can be improved. For stiffer applications, Hall effect sensors with up to 200 mV/mT sensitivity can be used, as mentioned in Section II-A. As only about 2.8V of the available 5V range are used, the signal could also be amplified. These modifications would reduce the noise levels. Furthermore, there are many possible non-linearities in the measurement including non-linear inter-axis coupling, anisotropic materials (such as 3D-printed PLA), and non-linear voltage response to changes in field for larger displacements or lateral and axial offsets. Hence, the simple linear calibration should be replaced by a neural network-based calibration as described in [39], where it was shown to lead to an order of magnitude decrease in error.

Other future work includes refinement and miniaturization of the electrical design, and integration into a 6-DOF sensor for an US probe and potentially other applications. This will enable data collection for AI and haptic feedback in US teleoperation systems. Generic placement of the sensors between a shell and the US probe will lead to an invertible matrix transforming sensing axes into overall rigid body resultants. This can be optimized by looking at the singular value decomposition of the matrix [40], with the possibility of preferential axes (e.g. axial force in the transducer imaging plane). In the presented tests, the sensors easily handled the manufacturing tolerances of an inexpensive 3D printer, so fabrication is easier than with many alternative methods. Furthermore, the modular nature of the sensor allows for communication with any microcontroller or interface, for example an ESP32 with Wi-Fi and Bluetooth capabilities or a custom-designed FPGA, and for flexible, optimizable positioning around the US probe.

Moreover, the sensor modules achieve the design goals of speed - the SPI throughput of 50 Mbps and ADC sampling rate of 100 kHz are more than sufficient - and cost. At a quantity of 10, the chosen ADC, Hall effect sensors, and magnets cost $4.77, $2.52, and $0.51 USD respectively. Thus, a sensor with six sensor modules would cost $61.91 plus fabrication which does not require costly degrees of precision.

V. Conclusion

This paper has introduced a novel concept for low-profile, low-cost multi-axis force sensing in relatively soft applications. Through initial experiments, the best-case deflection resolution is found to be 856 nm. With displacements of up to 1.1 mm for applied forces of 25 N and torques of 275 Nmm, the RMS error is 10.37%, which is just slightly above the human hand JND of 7%. Much future work is presented which can further improve performance and utility. By meeting the design goals set out in Section I-A, this sensor can enable haptic feedback and transparency in US teleoperation.

REFERENCES

[1] S. E. Salcudean, H. Moradi, D. Black, and N. Navab, "Robot-assisted medical imaging: A review," *Proceedings of the IEEE*, 2022.

[2] S. E. Salcudean, G. Bell, S. Bachmann, W.-H. Zhu, P. Abolmaesumi, and P. D. Lawrence, "Robot-assisted diagnostic ultrasound–design and feasibility experiments," in *International Conference on Medical Image Computing and Computer-Assisted Intervention*, pp. 1062–1071, Springer, 1999.

[3] M. Akbari, J. Carriere, T. Meyer, R. Sloboda, S. Husain, N. Usmani, and M. Tavakoli, "Robotic ultrasound scanning with real-time image-based force adjustment: Quick response for enabling physical distancing during the covid-19 pandemic," *Frontiers in Robotics and AI*, vol. 8, 2021.

[4] C. Delgorge, F. Courrèges, L. A. Bassit, C. Novales, C. Rosenberger, N. Smith-Guerin, C. Brù, R. Gilabert, M. Vannoni, G. Poisson, *et al.*, "A tele-operated mobile ultrasound scanner using a light-weight robot," *IEEE transactions on information technology in biomedicine*, vol. 9, no. 1, pp. 50–58, 2005.

[5] K. Mathiassen, J. E. Fjellin, K. Glette, P. K. Hol, and O. J. Elle, "An ultrasound robotic system using the commercial robot ur5," *Frontiers in Robotics and AI*, vol. 3, p. 1, 2016.

[6] D. Black, Y. Oloumi, A. H. H. Hosseinabadi, and S. Salcudean, "Human teleoperation - a haptically enabled mixed reality system for teleultrasound," *Human Computer Interaction*, 2022 (In press).

[7] D. Black and S. Salcudean, "A mixed reality system for human teleoperation in tele-ultrasound," pp. 91–92, Hamlyn Symposium for Medical Robotics, July 2022.

[8] O. Pallotta and A. Roberts, "Musculoskeletal pain and injury in sonographers, causes and solutions," *Sonography*, vol. 4, no. 1, pp. 5–12, 2017.

[9] T. Kaneko, N. Kagiyama, Y. Nakamura, T. Hirasawa, A. Murata, R. Morimoto, S. Miyazaki, and T. Minamino, "Effectiveness of real-time tele-ultrasound for echocardiography in resource-limited medical teams," *Journal of Echocardiography*, vol. 20, no. 1, pp. 16–23, 2022.

[10] K. Jemal, D. Ayana, F. Tadesse, M. Adefris, M. Awol, M. Tesema, B. Dagne, S. Abeje, A. Bantie, M. Butler, *et al.*, "Implementation and evaluation of a pilot antenatal ultrasound imaging programme using tele-ultrasound in ethiopia," *Journal of Telemedicine and Telecare*, p. 1357633X221115746, 2022.

[11] A. E. Drake, J. Hy, G. A. MacDougall, B. Holmes, L. Icken, J. W. Schrock, and R. A. Jones, "Innovations with tele-ultrasound in education sonography: the use of tele-ultrasound to train novice scanners," *The ultrasound journal*, vol. 13, no. 1, pp. 1–8, 2021.

[12] N. J. Soni, J. S. Boyd, G. Mints, K. C. Proud, T. P. Jensen, G. Liu, B. K. Mathews, C. K. Schott, L. Kurian, C. M. LoPresti, *et al.*, "Comparison of in-person versus tele-ultrasound point-of-care ultrasound training during the covid-19 pandemic," *The ultrasound journal*, vol. 13, no. 1, pp. 1–7, 2021.

[13] H. Sharma, L. Drukker, A. T. Papageorghiou, and J. A. Noble, "Multi-modal learning from video, eye tracking, and pupillometry for operator skill characterization in clinical fetal ultrasound," in *2021 IEEE 18th International Symposium on Biomedical Imaging (ISBI)*, pp. 1646–1649, IEEE, 2021.

[14] Z. Jiang, M. Grimm, M. Zhou, Y. Hu, J. Esteban, and N. Navab, "Automatic force-based probe positioning for precise robotic ultrasound acquisition," *IEEE Transactions on Industrial Electronics*, vol. 68, no. 11, pp. 11200–11211, 2020.

[15] S. Virga, O. Zettinig, M. Esposito, K. Pfister, B. Frisch, T. Neff, N. Navab, and C. Hennersperger, "Automatic force-compliant robotic ultrasound screening of abdominal aortic aneurysms," in *2016 IEEE/RSJ international conference on intelligent robots and systems (IROS)*, pp. 508–513, IEEE, 2016.

[16] L. Drukker, H. Sharma, R. Droste, M. Alsharid, P. Chatelain, J. A. Noble, and A. T. Papageorghiou, "Transforming obstetric ultrasound into data science using eye tracking, voice recording, transducer motion and ultrasound video," *Scientific Reports*, vol. 11, no. 1, p. 14109, 2021.

[17] R. Droste, L. Drukker, A. T. Papageorghiou, and J. A. Noble, "Automatic probe movement guidance for freehand obstetric ultrasound," in *Medical Image Computing and Computer Assisted Intervention–MICCAI 2020: 23rd International Conference, Lima, Peru, October 4–8, 2020, Proceedings, Part III 23*, pp. 583–592, Springer, 2020.

[18] T. Schimmoeller, R. Colbrunn, T. Nagle, M. Lobosky, E. E. Neumann, T. M. Owings, B. Landis, J. E. Jelovsek, and A. Erdemir, "Instrumentation of off-the-shelf ultrasound system for measurement of probe forces during freehand imaging," *Journal of biomechanics*, vol. 83, pp. 117–124, 2019.

[19] M. W. Gilbertson and B. W. Anthony, "An ergonomic, instrumented ultrasound probe for 6-axis force/torque measurement," in *2013 35th Annual International Conference of the IEEE Engineering in Medicine and Biology Society (EMBC)*, pp. 140–143, IEEE, 2013.

[20] M. O. Harris-Love, C. Ismail, R. Monfaredi, H. J. Hernandez, D. Pennington, P. Woletz, V. McIntosh, B. Adams, and M. R. Blackman, "Interrater reliability of quantitative ultrasound using force feedback among examiners with varied levels of experience," *PeerJ*, vol. 4, p. e2146, 2016.

[21] G. P. Mylonas, P. Giataganas, M. Chaudery, V. Vitiello, A. Darzi, and G.-Z. Yang, "Autonomous efast ultrasound scanning by a robotic manipulator using learning from demonstrations," in *2013 IEEE/RSJ International Conference on Intelligent Robots and Systems*, pp. 3251–3256, IEEE, 2013.

[22] Q. Huang, J. Lan, and X. Li, "Robotic arm based automatic ultrasound scanning for three-dimensional imaging," *IEEE Transactions on Industrial Informatics*, vol. 15, no. 2, pp. 1173–1182, 2019.

[23] Y. Wei and Q. Xu, "An overview of micro-force sensing techniques," *Sensors and Actuators A: Physical*, vol. 234, pp. 359–374, 2015.

[24] J. O. Templeman, B. B. Sheil, and T. Sun, "Multi-axis force sensors: A state-of-the-art review," *Sensors and Actuators A: Physical*, vol. 304, p. 111772, 2020.

[25] C. Lebossé, P. Renaud, B. Bayle, and M. de Mathelin, "Modeling and evaluation of low-cost force sensors," *IEEE Transactions on Robotics*, vol. 27, no. 4, pp. 815–822, 2011.

[26] Y.-L. Park, B.-R. Chen, and R. J. Wood, "Design and fabrication of soft artificial skin using embedded microchannels and liquid conductors," *IEEE Sensors journal*, vol. 12, no. 8, pp. 2711–2718, 2012.

[27] A. H. H. Hosseinabadi, M. Honarvar, and S. E. Salcudean, "Optical force sensing in minimally invasive robotic surgery," in *2019 International Conference on Robotics and Automation (ICRA)*, pp. 4033–4039, IEEE, 2019.

[28] A. H. H. Hosseinabadi, D. Black, and S. E. Salcudean, "Ultra low-noise fpga-based six-axis optical force–torque sensor: Hardware and software," *IEEE Transactions on Industrial Electronics*, vol. 68, no. 10, pp. 10207–10217, 2020.

[29] S. A. Liu and H. L. Tzo, "A novel six-component force sensor of good measurement isotropy and sensitivities," *Sensors and Actuators A: Physical*, vol. 100, no. 2-3, pp. 223–230, 2002.

[30] B.-Y. Lee, J. Kim, H. Kim, C. Kim, and S.-D. Lee, "Low-cost flexible pressure sensor based on dielectric elastomer film with micro-pores," *Sensors and Actuators A: Physical*, vol. 240, pp. 103–109, 2016.

[31] D. Jones, L. Wang, A. Ghanbari, V. Vardakastani, A. E. Kedgley, M. D. Gardiner, T. L. Vincent, P. R. Culmer, and A. Alazmani, "Design and evaluation of magnetic hall effect tactile sensors for use in sensorized splints," *Sensors*, vol. 20, no. 4, p. 1123, 2020.

[32] P. J. Kyberd and P. H. Chappell, "A force sensor for automatic manipulation based on the hall effect," *Measurement Science and Technology*, vol. 4, no. 3, p. 281, 1993.

[33] H. Kristanto, P. Sathe, A. Schmitz, T. P. Tomo, S. Somlor, and S. Sugano, "A wearable three-axis tactile sensor for human fingertips," *IEEE Robotics and Automation Letters*, vol. 3, no. 4, pp. 4313–4320, 2018.

[34] S. D. M. Nasab, A. Beiranvand, M. T. Masouleh, F. Bahrami, and A. Kalhor, "Design and development of a multi-axis force sensor based on the hall effect with decouple structure," *Mechatronics*, vol. 84, p. 102766, 2022.

[35] H. Z. Tan, M. A. Srinivasan, B. Eberman, and B. Cheng, "Human factors for the design of force-reflecting haptic interfaces," *Dynamic Systems and Control*, vol. 55, no. 1, pp. 353–359, 1994.

[36] D. B. Kaber and T. Zhang, "Human factors in virtual reality system design for mobility and haptic task performance," *Reviews of Human Factors and Ergonomics*, vol. 7, no. 1, pp. 323–366, 2011.

[37] S. A. Wall and W. Harwin, "A high bandwidth interface for haptic human computer interaction," *Mechatronics*, vol. 11, no. 4, pp. 371–387, 2001.

[38] N. Derby and S. Olbert, "Cylindrical magnets and ideal solenoids," *American Journal of Physics*, vol. 78, no. 3, pp. 229–235, 2010.

[39] A. Hadi-Hosseinabadi and S. Salcudean, "Multi-axis force sensing in robotic minimally invasive surgery with no instrument modification," *arXiv preprint arXiv:2103.11116*, 2021.

[40] A. Bicchi, "A criterion for optimal design of multi-axis force sensors," *Robotics and Autonomous Systems*, vol. 10, no. 4, pp. 269–286, 1992.